A Multisensor Approach to Dust Storm Monitoring Over the Nile Delta

Hesham M. El-Askary, Sudipta Sarkar, Menas Kafatos, *Member, IEEE*, and Tarek A. El-Ghazawi, *Senior Member, IEEE*

***Abstract*—This work analyzes several remote sensing instrument capabilities in monitoring dust storms. Multisensor data analysis is carried out to study the behavior of dust particles at different wavelengths. A technique based on a combination of optical and microwave sensing of dust storms, using the Moderate Resolution Imaging Spectrometer (MODIS) and the Tropical Rainfall Measuring Mission (TRMM) Microwave Imager (TMI) respectively, is found to be particularly useful.**

***Index Terms*—Aerosol index, brightness temperature, dust storm, Nile Delta, scattering coefficient, urban areas.**

I. Introduction

THE NILE Delta is often subjected to dust storms that originate in the Sahara. Such storms blow across the north and northeast directions toward the Mediterranean Sea and the Arabian Peninsula. Occasionally, dust storms can travel all the way to North America. In the summer months, these dust storms have a significant impact on the amount of solar radiation that reaches the surface, producing a cooling effect that can reach North America [1]. Sand and dust stirred up by winds can trigger blinding dust storms causing near-zero visibility conditions. Such dust storms can also pose a serious health risk for people with respiratory disorders. Hence, it is imperative to be able to monitor dust storms and predict their evolution. Little work, however, has been done on integrated multisensor detection of dust storms. Furthermore, earlier work [2] has produced some results based on an array of optical sensors but did not focus much on the microwave range of the spectrum. This can lead to confusing dust storms with other phenomena such as clouds. In this paper, we focus on two sensors that we believe are best suited for detection of dust storms. These are the Moderate Resolution Imaging Spectroradiometer (MODIS) and the Tropical Rainfall Measuring Mission (TRMM) Microwave Imager (TMI).

II. Sensors and Data for Dust Storm Detection

Many remote sensing systems can be used for detecting dust storms. Geostationary Operational Environmental Satellites (GOES) are considered to be the most suitable systems to track the time evolution of active and short lived dust storms because of their high temporal resolution (15 min). This is because of the fact that suspended dust is highlighted against the background as brightness changes. However, due to the poor spatial (1 km) and spectral (1-visible) resolutions, it is used only to detect and monitor very large dust storms [3]. On the other hand, Landsat TM has very good spatial resolution. Therefore, it can map the dust source location accurately if the image is cloud-free. However, it is subjected to poor temporal resolution (two weeks) and just like GOES, has inherent difficulty in penetrating clouds [3]. Sea-viewing Wide Field of view Sensor (SeaWiFS) is a useful sensor in detecting dust plumes lasting for a long period of time and having a dark (low-radiance) background (i.e., the ocean) [3]. It has been used to detect the very large dust plumes generated by winds in Africa and Asia [4], [5]. However, SeaWiFS may have difficulty detecting small and short-lived dust events over desert areas, due to their high-radiance [3]. The Total Ozone Mapping Spectrometer (TOMS) can be used in the ultraviolet range. However, TOMS data may produce misleading results by confusing dust with aerosol particles. This is because the TOMS sensor responds to backscattered radiation caused by Rayleigh scattering when particles are smaller than the incident wavelength. Dust particles are, however, coarser and more likely to produce Mie scattering.

Our approach puts more weight on the usage of MODIS and TMI. MODIS has good spectral resolution with its 36 channels spanning the visible (0.415 μm) to the thermal infrared (14.235 μm) spectrum. Furthermore, it has fair spatial resolution that ranges from 250 m to 1 km at nadir. It also has good temporal repeativity of twice a day, using Terra MODIS and Aqua MODIS. MODIS data were found to be suitable for monitoring environmental changes [6]. This study makes use of the MODIS level 1B radiance and the MODIS Level 2 daily 5-min water vapor data to identify and delineate dust storms. At the other end of the spectrum, we utilize passive microwave data from TMI. This allows efficient estimation of the scattering produced by dust particles that have high single-scattering albedo. We have used TMI microwave brightness temperature data to deduce information about the scattering characteristics of dust particles. Such particles have a high single-scattering albedo over a given study area. In addition, the TMI hydrometeor profile data are used to show the buildup of water vapor concomitants into dust storms that prevent solar radiation from arriving to the land surface. In previous work TRMM data showed that dust storms can amplify desertification effects [7]. Data used in this analysis are

Manuscript received February 10, 2003; revised June 24, 2003.

H. M. El-Askary, S. Sarkar, and M. Kafatos are with the Center for Earth Observing and Space Research (CEOSR), George Mason University (GMU), Fairfax, VA 22030 USA (e-mail: helaskar@scs.gmu.edu; ssarkar@gmu.edu; mkafatos@gmu.edu).

T. A. El-Ghazawi is with the School of Engineering and Applied Science, George Washington University, Washington DC 20052 USA (e-mail: tarek@sea.gwu.edu).

Digital Object Identifier 10.1109/TGRS.2003.817189

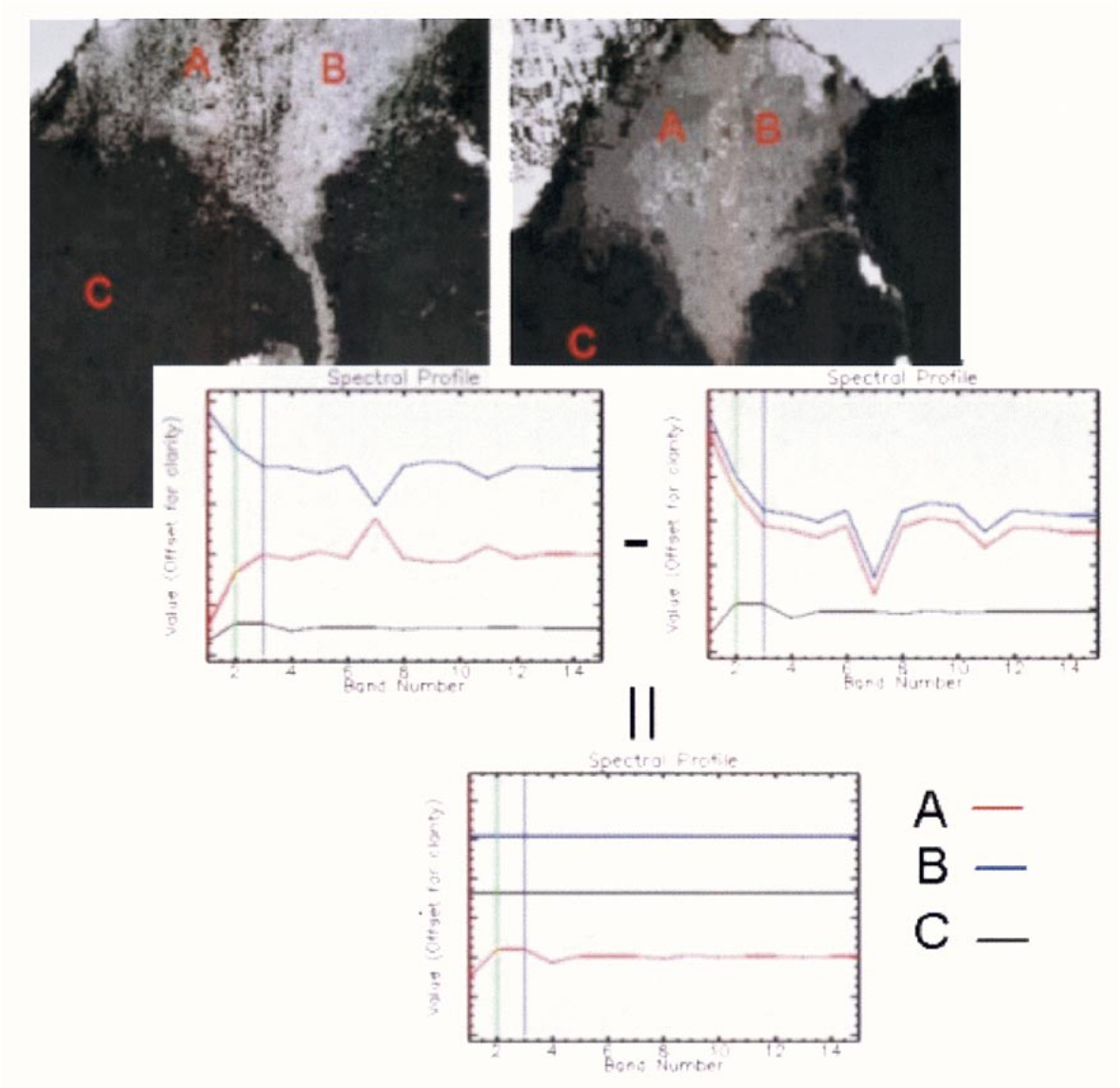

Fig. 1. MODIS grayscale first principal component for the dust storms (of September 1 and 3) and the associated spectral patterns obtained from the original bands. (Upper graphs, top to bottom) B (blue), A (red), C (black). (Lower graph, top to bottom) B (blue), C (black), and A (red). The x axis shows band number (0–14). The y axis shows value (offset for clarity).

in the period from late August to early September 2000, at which time a major dust storm over Nile Delta took place. This was an unusual time for a dust storm occurrence, as the dust storm season is generally late spring.

III. Monitoring Dust Storms in the Visible Range

The MODIS level 1B radiance dataset contains the radiance counts from 36 spectral bands. To extract meaningful information and to reduce the dimensions, a spectral principal component analysis (PCA) is applied. PCA is a coordinate transformation typically associated with multiband imagery. PCA reduces data redundancy by creating a new series of images (components) in which the axes of the new coordinate system point in the direction of decreasing variance. For more details on PCA, interested readers can consult [8]. The MODIS radiance bands from September 1 and 3, 2000, were transformed in the above manner. The first four principal components (PCs) for each day are found to contain about 90% of the total variance. From the first PC for both days, it was clear that the western part of the Nile Delta was showing the presence of strange features on September 1. We suspected such features to be dust since they totally disappeared on September 3. To study these features, three locations were selected over the Western Desert and the Nile Delta, from September 1 and 3. Spectral patterns are observed and averaged over a 5×5 window in these locations. The spectral patterns of these three regions on September 1 totally differ. This is because they represent vegetation mixed with dust, pure vegetation, and pure dust in regions "A," "B," and "C," respectively. The difference in the spectral signatures of regions "A" and "B" is the result of light scattered from the suspended dust that does not entirely reach the ground. Therefore vegetation does not absorb all the radiation coming from the sun as some radiation is scattered back to the sensor without reaching the ground. On September 3, the spectral patterns of regions "A"

and "B" agree with each other, as they both represent pure vegetation. The signature of region "C" appears the same on both days, as it represents dust in the Western Desert. By calculating the spectral difference between the three patterns for September 1 and 3, Regions "B" and "C" produce a zero difference, as they have not changed over the two days. However, region "A" shows a difference that matches very well the pattern obtained from region "C" in both days, which corresponds to pure dust. This suggests the occurrence of dust storms, over the Nile Delta that had transported from the Western Desert. The two figures for the first PC for September 1 and 3, and the selected locations over which the spectral patterns were obtained, are shown in Fig. 1. We stacked our data and set an offset distance for the clarity of different spectral profiles of the three different locations.

In Fig. 1, band 7 falls in the shortwave infrared (SWIR) region of the spectrum while band 11 falls in the green portion of the spectrum. Saharan dust is mainly composed of silica particles that produce a high peak in the SWIR region, and a well-known reflectance albedo over the green region of the visible spectrum. This explains the presence of the high peaks over bands 7 and 11. However the pure vegetation signature taken from region "B" shows a minimum over the SWIR region as the plants do not have enough water supplies. Hence the cells of the leaves get smaller and the cell structure changes. This leads to less reflection in the near infrared and significantly less in the short wave infrared compared with healthy vegetation.

For further verification of the presence of the Sahara dust over the Nile Delta and the Mediterranean, the first four PCs were subjected to a K-means clustering analysis. The applied K-means algorithm in this study uses the spectral properties of the multispectral image for clustering. K-means produces a partition of a discrete set of objects into a smaller discrete set of classes. The algorithm was implemented with 4 classes, for a total of 20 iterations. The classified principal component image is shown in Fig. 2. This figure shows that the dust particles over the Nile Delta belong to the same class as the Western desert.

Dust plumes are three-dimensional features and characterized by vertical and horizontal motion. The specific direction and trend of dust storms can be clearly delineated and identified with the use of directional filters. Therefore, we applied a 3 $\times$ 3 kernel *Sobel filter* [9] to distinguish the abnormal concentrations of dust clouds and specify their direction over the Nile Delta. Sobel filter operates by estimating the magnitude of the directional derivatives along any two given directions. The directions have been preset along the horizontal and the vertical orientations. The two kernels that detect horizontal and vertical changes in the image, Gx and Gy, are shown in (1), [9]

$$\left.\begin{aligned} G_X &= F_{j+1,k+1} + 2F_{j+1,k} + F_{j+1,k-1} \\ &\quad -(F_{j-1,k+1} + 2F_{j-1,k} + F_{j-1,k-1}) \\ G_Y &= F_{j-1,k-1} + 2F_{j,k-1} + F_{j+1,k-1} \\ &\quad -(F_{j-1,k+1} + 2F_{j,k+1} + F_{j+1,k+1}) \end{aligned}\right\}. \tag{1}$$

The final output G_{jk} is the sum of changes in magnitude of the edges in the two direction images as shown in (2)

$$G_{jk} = |G_X| + |G_Y| \tag{2}$$

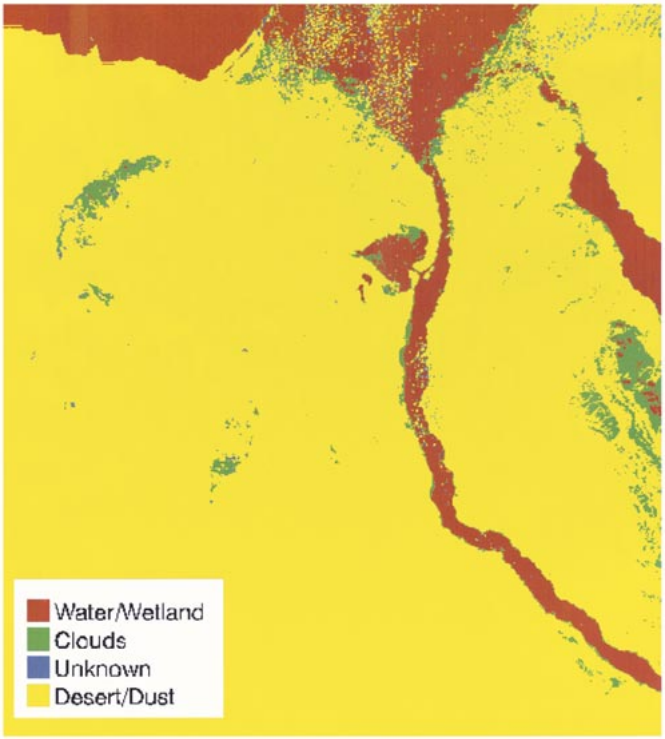

Fig. 2. K-means classification of the first four principal components of September 1, 2000.

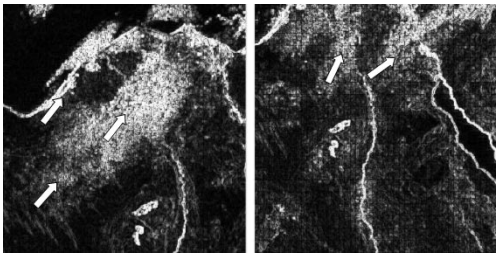

Fig. 3. Two Sobel filtered images from (left) August 31 and (right) September 1, 2000, showing the general direction of the dust storm over the Nile Delta.

where (j,k) are the coordinates of each pixel F_{jk} in the image.

The advantage of this filter is that it is able to capture the changes in the image in two dimensions as shown in Fig. 3.

From the previous figure, it is clear that the dust storm drifted away from the Western Desert toward the Nile Delta on August 31. On September 1, it started drifting away from the western part of the Nile Delta. This direction of the dust cloud matches the known direction of winds prevailing during September, namely from the south to the southwest direction [10].

IV. Microwave Sensing of Dust Storms

The presence of the dust storm over the Nile Delta has been corroborated through the use of passive microwave data. The single-scattering albedo over optical wavelengths is different from the microwave. Over the microwave range the single-scattering albedo plays a more important role than the emissivity of

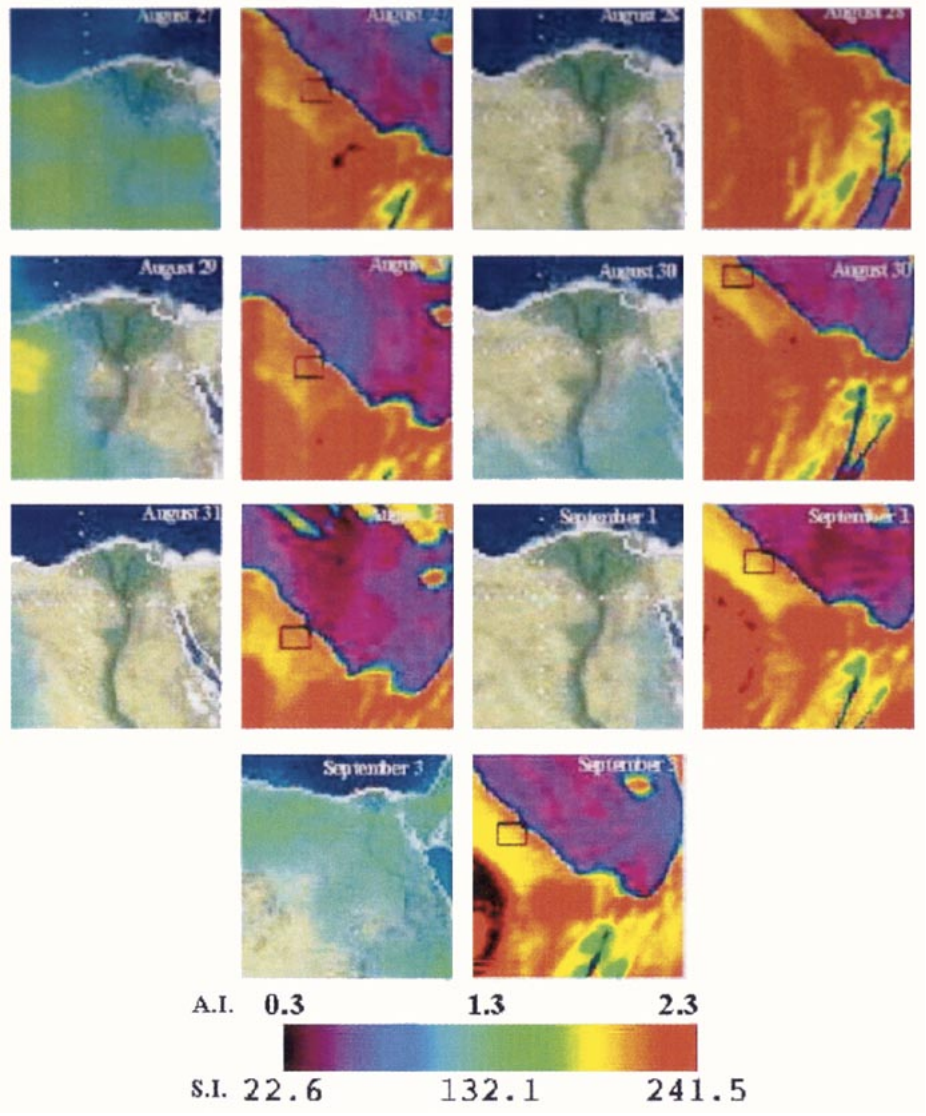

Fig. 4. Variation of the scattering index and aerosol index derived from TMI brightness temperatures and TOMS shown side by side, (left) TOMS and (right) TMI in each image pair.

the medium through which the radiation passes. The single-scattering albedo is defined as the probability that given an interaction between the photon and a particle, the particle will be scattering rather than absorbing. For a single particle size, this probability may easily be expressed in terms of the optical efficiencies as shown in (3) where, (τ_e) is the extinction coefficient and (τ_a) is the absorption coefficient [11]

$$\overline{\omega} = \frac{1 - \tau_a(r, \lambda)}{\tau_e(r, \lambda)}. \tag{3}$$

Dust particles are of a larger dimension than the normal aerosol particulates, but are of similar size to the incident microwave radiation. Therefore, microwave radiation responds to dust particles with Mie scattering. The shorter the wavelength of the incident radiation in the microwave range, the greater is the scattering and hence the lower the brightness temperature is. For quantitative estimation of the amount of scattering produced by dust particles suspended over the Nile Delta, in the 85-GHz vertically polarized channel, the brightness temperature over 19- and 22-GHz vertical channels

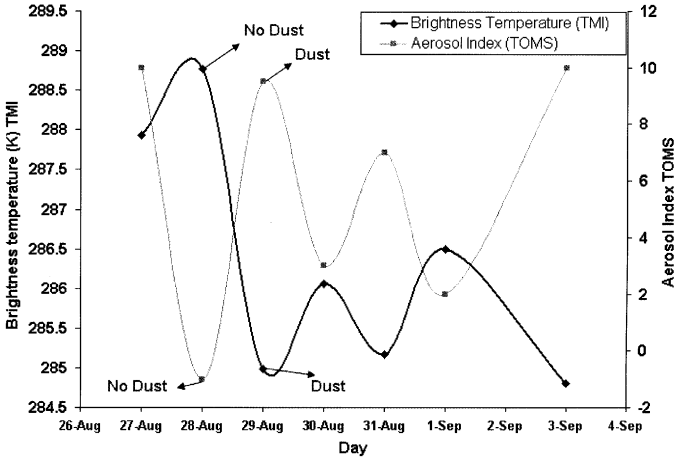

Fig. 5. Daily variations of brightness temperature and aerosol index for the selected areas in Fig. 4.

TABLE I

Sensor	Wavelength Range	Used Parameter	Strength towards Dust Storm Detection
TOMS	Ultra Violet	UV backscattered radiation	Not very efficient for detecting coarse grained storms
MODIS	Visible, IR	Reflectance and water vapor	Efficient detection of dust storms from their high albedo and attendant smog formation
TMI	Microwave	Brightness Temperature, Mie scattering	Penetrates cloud and detects dust through backscattered radiation in microwave range

were integrated and the 85-GHz response was subtracted from them. This approach uses the single-scattering albedo in (3) and has been described in [12] and shown in (4)

$$SI_{85} = 451.9 - 0.44^{*}TB_{19V} - 1.775^{*}TB_{22V} + 0.005\,74^{*}TB_{22V}{}^{*}TB_{22V} - TB_{85V} \quad (4)$$

where TB refers to the brightness temperature over the specific channel, and SI_{85} is the scattering index (SI) derived for the 85 GHz. The SI shows an increase with greater scattering, and leads to a decrease in brightness temperature. The drop in brightness temperature results as less radiation reaches the sensor in the shorter wavelengths due to greater scattering.

The SI has been calculated for a number of days starting from August 27 to September 3. Brightness temperature is averaged for the Nile Delta over a 20×20 window, for all the days for which the SI was estimated, as shown in Fig. 4. The black square in each of them represents the area over which the 20×20 window has been averaged. The TOMS derived aerosol index (AI) scenes[1] are shown side by side with our TMI figures for comparison; see Fig. 4.

The daily variations of brightness temperature (TMI) were plotted against the AI (TOMS), for the marked region in Fig. 4. Low brightness temperature days that correspond to greater scattering produced by dust particles are shown in brighter color within the blue to yellow range in Fig. 4. A bright color (yellow) indicates the increasing presence of dust. A clear correspondence between the scattering and microwave brightness temperature emerges, as the dust storm is seen to oscillate and migrate over our study area. Furthermore, a significant negative correlation ($r = -0.56$, p-value $= 0.0175$ from the two-tailed t-test) between the ultraviolet derived TOMS AI and the microwave derived TMI brightness temperature is observed. Such relation corresponds to the variation in the scattering property of the surface and is noteworthy as shown in Fig. 5.

The days having higher values of AI as obtained from TOMS show lower brightness temperature and are indicated by yellow color in Fig. 4. The TOMS product is derived from the ultraviolet spectral region and captures the response of smaller particles namely aerosol to Rayleigh scattering, which is prominent at a relatively longer wavelength, compared to particle size. In the microwave range—namely, TMI—the wavelength is significantly larger. Therefore, Mie scattering applies when sand particles are about the same size as the radiation wavelength. In this respect, the microwave is far more suitable than the ultraviolet range as it may not differentiate dust particles from aerosols. Moreover, as the size of dust particles is substantially larger than aerosol particulates, they are not amenable to proper monitoring by optical sensors. Note that in [13] it was estimated that the sand grain size (diameter), is ranging from 2–1/16 mm, whereas the silt size is 1/16 to 1/32, and the clay size can be from 1/32 to 1/264. So, the expected grain size of the dust settled at the higher levels of the atmosphere ranges from fine sand to clay.

Dust storms can be monitored also by looking at their effect on water vapor. The dust particles act as a small cloud condensation nucleus, around which water vapor droplets can accrete and give rise to smog and fog. The strength of the different sensors used in this study for dust storm detection is summarized in Table I.

[1]TOMS Data Source at Goddard Daac. See http://jwocky.gsfc.nasa.gov/aerosols/today_plus/yr2000/images_2000.html.

V. Conclusion

Dust storms can vary in coverage, particle size, distribution, and direction. We utilized the difference in behavior between dust and haze in different regions of the electromagnetic spectrum in order to detect and track dust storms. In the optical part of the spectrum, dust storms have a very high albedo and hence appear quite bright. Therefore, one can look for high reflectance and anomalous water vapor to serve as indicators of dust storms. In the longer wavelength microwave region, dust storms respond strongly to scattering and this leads to reduced brightness temperature. We believe that a combined approach of optical and microwave sensing is best suited to monitoring and tracking dust storms. This can also help distinguish dust storms from aerosol particles, which is an advantage over using TOMS alone. Thus, a multisensor approach to monitoring and tracking dust storms can be quite useful.

References

[1] B. G. Liepert, "Observed reductions of surface solar radiation at sites in the United States and worldwide from 1961 to 1990," *Geophys. Res. Lett.*, vol. 29, no. 10, May 2002.

[2] D. J. MacKinnon and P. S. Chavez, Jr., "Dust storms," *Earth Mag.*, pp. 60–64, 1993.

[3] P. S. Chavez, D. J. Mackinnon, R. L. Reynolds, and M. G. Velasco, "Monitoring dust storms and mapping landscape vulnerability to wind erosion using satellite and ground-based digital images," *Aridlands News Lett.*, no. 51, May/June 2002.

[4] J. M. Prospero, "Long-range transport of mineral dust in the global atmosphere: impact of African dust on the environment of the Southeastern United States," in *Proc. Nat. Acad. Sci.*, vol. 96, 1999, pp. 3,396–3,403.

[5] R. B. Husar, D. M. Tratt, B. A. Schichtel, S. R. Falke, F. Li, D. Jaffe, S. Gasso, T. Gill, N. S. Laulainen, F. Lu, M. C. Reheis, Y. Chun, D. Westphal, B. N. Holben, C. Gueymard, I. McKendry, N. Kuring, G. C. Feldman, C. McClain, R. J. Frouin, J. Merrill, D. DuBois, F. Vignola, T. Murayama, S. Nickovic, W. E. Wilson, K. Sassen, N. Sugimoto, and W. C. Malm, "Asian dust events of April 1998," *J. Geophys. Res.*, vol. 106, pp. 18 317–18 330.

[6] H. El-Askary, M. Kafatos, and M. Hegazy, "Environmental monitoring of dust storms over the Nile Delta, Egypt using MODIS satellite data," in *Proc. 3rd Int. Symp. Remote Sensing of Urban Areas*, Istanbul, Turkey, June 2002.

[7] D. Rosenfeld, "Smoke and desert dust stifle rainfall, contribute to drought and desertification," *Aridlands News Lett.*, no. 49, May/June 2001.

[8] I. Joliffe, *Principal Component Analysis*. Berlin, Germany: Springer, 1986.

[9] J. A. Richards and X. Jia, *Remote Sensing Digital Image Analysis: An Introduction*. Berlin, Germany: Springer-Verlag, 1999.

[10] Egyptian Meteorological Authority, Climatic Atlas of Egypt, Cairo, Egypt, 1996.

[11] C. Zender, "Radiative transfer in the earth system,", GNU Free Doc. License.

[12] R. R. Ferraro and N. C. Grody, "Effects of surface conditions on rain identification using the DMSP-SSM/I," *Remote Sens. Rev.*, vol. 11, pp. 195–209, 1994.

[13] C. K. Wentworth, "A scale of grade and class terms for clastic sediments," *J. Geol.*, vol. 30, pp. 377–392, 1922.